Anal. Methods Environ. Chem. J. 8 (1) (2025) 39-53

AMECJ

Research Article, Issue 1
Analytical Methods in Environmental Chemistry Journal
Journal home page: www.amecj.com/ir

Electrochemical Spectroscopy: Evaluation and determination of Carbon dioxide reduction based on tin oxide doped ethyl cellulose as electrocatalyst by H-type cell and reversible hydrogen electrode

Ali Hussein Ghanim[a, *] **and Khulood Abid Salah**[b]
[a]*University of Baghdad, Collage of Science, Chemistry Department, Iraq*
[b]*University of Baghdad, Collage of Science, Chemistry Department, Iraq*

ARTICLE INFO:
Received 17 Nov 2024
Revised form 2 Feb 2025
Accepted 26 Feb 2025
Available online 28 March 2025

Keywords:
CO_2 reduction,
Catalyst,
Tin oxide,
Electrochemical spectroscopy,
Electrocatalytic reduction

ABSTRACT
Electrocatalytic Carbon dioxide (CO_2) reduction to carbon products on SnO_2-doped ethyl cellulose (EC) was prepared by dispersion of nano-sized tin oxide (SnO_2, 25 nm) in ethyl cellulose through sonication by an ultrasonic probe (600 W) for 60 min. The SnO_2-EC catalyst is characterized by field emission scanning electron microscopy (FESEM), atomic force microscopy (AFM), and X-ray diffraction (XRD). The electrocatalytic performance for CO_2 reduction was investigated by loading SnO_2-EC paste on a 306S.S. rotated disc. The CO_2 electroreduction occurred in an H-type cell with three electrodes in 0.1M $KHCO_3$ saturated with CO_2 at different potential ranges of -1.0 V to -1.8V vs. reversible hydrogen electrode (RHE) for 3 hours. The oxygen content of liquid products was collected and determined using a chemical oxygen demand (COD,15–300 mg L^{-1}) kit, which was quantified by a colorimeter. A higher oxygen content concentration was obtained at -1.2V vs. RHE (-2 mA cm^{-2}) and found to be 235 mg L^{-1}, while the oxygen content tends to decrease with a more negative applied potential of -1.4V, -1.6V, and 1.8V vs. RHE with current densities of -2.5 mA cm^{-2}, -7.3 mA cm^{-2}, and -15.6 mA cm^{-2}, respectively.

1. Introduction

The scientific community attributes the causes of climate change to the increased production of carbon dioxide (CO_2) through human activity. CO_2 is one of the principal greenhouse gases contributing to global warming. To minimize the continuous growth of its atmospheric concentration, CO_2 can be used as raw material to obtain products with high energy value [1]. Electrochemical CO_2 reduction reaction (CO_2RR) is recognized as one of the most attractive and environmentally friendly approaches for reducing CO_2 emissions. This approach is especially effective when integrated with the utilization of renewable energies [2-3]. Carbon dioxide (CO_2) is a highly stable molecule that requires considerable energy to transform into useful compounds. Scientists have identified several methods to convert CO_2 into valuable chemicals, including carbon monoxide (CO) [4]. hydrocarbons, and oxygenated hydrocarbons. These methods include gas-phase, liquid-phase, electrochemical, and photocatalytic reactions. Gas-phase reactions involve dry reforming of methane ($CH_4 + CO_2 \rightarrow 2CO + 2H_2$) and hydrogenation of CO_2 ($CO_2 + H_2 \rightarrow CO + H_2O$, which is also known as the water-gas shift reversal reaction; $CO_2 + 4H_2 \rightarrow CH_4 + 2H_2O$). On the other hand, the liquid-phase technique uses CO_2 dissolved

*Corresponding Author: Ali Hussein Ghanim
Email: ali.ghanem@sc.uobaghdad.edu.iq
https://doi.org/10.24200/amecj.v8.i01.364

in an aqueous solution ($CO_{2(aq)} + H_{2(aq)} \rightarrow COOH$) to produce formic acid (HCOOH) [4–8]. Carbon dioxide (CO_2) electroreduction is a process that involves different numbers of electrons and protons to produce specific products. Metallic catalysts such as gold (Au), silver (Ag), palladium (Pd), zinc (Zn), lead (Pb), bismuth (Bi), tin (Sn), indium (In), mercury (Hg), and copper (Cu) have shown remarkable selectivity towards different products. Depending on the catalyst used, the major products of CO_2 electroreduction can be classified into three categories: (1) CO is produced by Au, Ag, Pd, and Zn; (2) formic acid/formate is produced by Pb, Bi, Sn, In, and Hg; [9–11] (3) various hydrocarbons are produced by Cu [12–15]. Despite this promising progress, these catalysts are still far from being industrially applicable, especially regarding current density. To have a sustainable impact on the environment and climate, it is crucial to conduct industrially relevant research. Therefore, urgent efforts are needed to develop more efficient and cost-effective catalysts for CO_2 electroreduction [16]. The CO2 reduction reaction (CO2RR) process faces challenges such as high overpotential and low current density [17-18]. Additionally, if the reaction occurs in an aqueous solution, the hydrogen evolution reaction competes with the desired product formation [19]. Therefore, the selectivity of product formation is influenced by several factors, such as the concentration of CO_2 in the electrolyte, electrode potential, temperature, electrolyte solution, and electrocatalyst used [15]. Electrocatalytic reduction of CO_2, also known as CO_2RR, is a challenging process due to the thermodynamic stability of CO_2, which causes slow reaction kinetics. Moreover, CO_2 conversion often competes with hydrogen evolution reaction (HER), leading to reduced selectivity of carbon products. Therefore, there is a need for highly effective, selective, and stable electrocatalysts to meet the requirements for practical applications of CO_2RR [20]. In electrocatalysis, several techniques have been developed to improve the performance of catalysts. These methods include alloying, surface modification, element doping, oxidative treatment, and shape control [21]. Alloying is widely regarded as one of the most effective ways to enhance electrocatalytic activity. This is because bimetallic alloying can modify not only the conventional electronic and geometric structures but also the ensemble effects of the metal active sites. By introducing a second metal into the catalyst, alloying can create new active sites or modify the electronic properties of existing sites, leading to improved catalytic activity and selectivity. Overall, alloying as a strategy for enhancing electrocatalytic performance has shown great promise in many research studies [22-23]. Tin (Sn) based catalysts have recently emerged as a promising metal for catalyzing the electrochemical reduction of CO_2. These are highly efficient, selective, and cost-effective, making them an attractive alternative to noble metal-based catalysts [24]. Sn-based catalysts can selectively convert CO_2 to formate, a valuable chemical feedstock. A wide range of Sn-based catalysts has been reported for CO2RR, including single metals, alloys, oxides [25,26], sulfides, and hybrids with carbon nanomaterials such as carbon nanotubes and graphene. These hybrids offer improved catalytic activity and stability and enhanced selectivity towards formate production. Furthermore, Sn-based catalysts are eco-friendly, non-toxic, and abundant in nature, making them a sustainable alternative to traditional catalysts. Currently, formate and CO can achieve Faradaic efficiencies of ~ 100% and over 90%, respectively [27-31]. We experimented to test the effectiveness of adding ethyl cellulose (EC) to SnO_2 nanoparticles (NPs) and applying it onto a rotated disk of 306 stainless (306S.S) steel using the drop-casting technique. The resulting SnO_2-EC@306S.S electrode was used as a catalyst for CO_2 reduction. Ethylcellulose helps to improve the adhesion of SnO_2 NPs to the substrate and prevent degradation. We analyzed the structure and composition of the SnO_2-EC@306S.S electrode using various methods, including atomic force microscopy (AFM), Field emission scanning electron microscopy (FESEM), X-ray diffraction (XRD), and Fourier transform infrared spectroscopy (FT-IR). To evaluate the catalyst's efficiency in promoting the reduction of CO_2, we used an H-type cell equipped with three electrodes and a solution of 0.1M $KHCO_3$ with a continuous flow of CO_2 gas. We applied a negative potential ranging from -1.8V to -1V at intervals of 0.2V. The CO_2 liquid products were

analyzed using the chemical oxygen demand (COD) method, and it was found that the oxygen content reached a maximum value of 226 mgL^{-1} at a potential of -1.2 mV.

2. Material and Methods

2.1. Reagents

Tin oxide nanoparticles (SnO_2 NPs, 305nm, CAS No:18282-10-5) were purchased from Hongwu International Group, China. At the same time, ethyl cellulose (EC, 99%, CAS No:9004-57-3) was procured from Sigma Aldrich, Germany. Potassium hydrogen carbonate ($KHCO_3$, 99.99%, CAS No:298-14-6) was prepared from Fluke, Germany. Nafion (5 wt.%, CAS No:31175-20-9) solution was purchased from Wuhan Golden Kylin industry, and Ethanol (EtOH, 99.9%, CAS No:64-17-5) was purchased from Chem-lab company, Belgium. The carbon dioxide (CO_2, 99.999%, CAS No:124-38-9) and Nitrogen gas (N_2, 99.999%, CAS No:7727-37-9) supplied Gulf company for industrial gases, Baghdad, Iraq.

2.2. Characterization instruments

Field Emission-Scanning Electron Microscope (FE-SEM, Sigma VP-Zeiss equipped with EDS-EBSD-Mapping-Line, Oxford Instrument Co) was used to examine the morphology of SnO_2 and EC-SnO_2 catalysts. Additionally, an Atomic Force Microscope (CoreAFM, Nanosurf, Switzerland) was used to measure the coated catalyst's particle size, roughness, adhesion force, and hardness. XRD diffraction (PANalytical XPert Pro XRD, Philips, Holland) was employed to estimate grain size, and electrocatalytic CO_2 reduction was carried out using the Vertex One Potentiostat equipped with Electrochemical Impedance Spectroscopy (EIS, Ivium Technologies, Holland). Finally, a Colorimeter (Lovibond, Germany) was employed to measure COD content.

2.3. Preparation of SnO_2-Doped Ethyl Cellulose (SnO_2-EC)

In a one-neck round-bottom flask (25 mL), 8 mg of ethyl cellulose (EC) was dissolved in 20 mL of ethanol and sonicated for 30 min. Then, 92 mg of SnO_2 NPs was added to the solution, and the mixture was stirred at room temperature for 120 min. After that, the solution was concentrated by evaporating the solvent at 50°C for 60 min. The thick solution was decanted into a Petri dish, and the yellow powder was collected and dried at 60°C for 10 hours. The resultant composite was donated as SnO_2-EC.

2.4. Preparation of Working Electrode (SnO_2-EC@306S.S)

To prepare the catalyst, 50 mg of SnO_2-EC powder was mixed with 500 µL ethanol and 100 µL Nafion (5 wt.%). An ultrasonic probe sonicated the mixture for 10 minutes, after which thick ink dropped-casted onto a rotating disc of 1 cm^2 306 stainless steel and allowed to dry at room temperature, as illustrated in Figure 1.

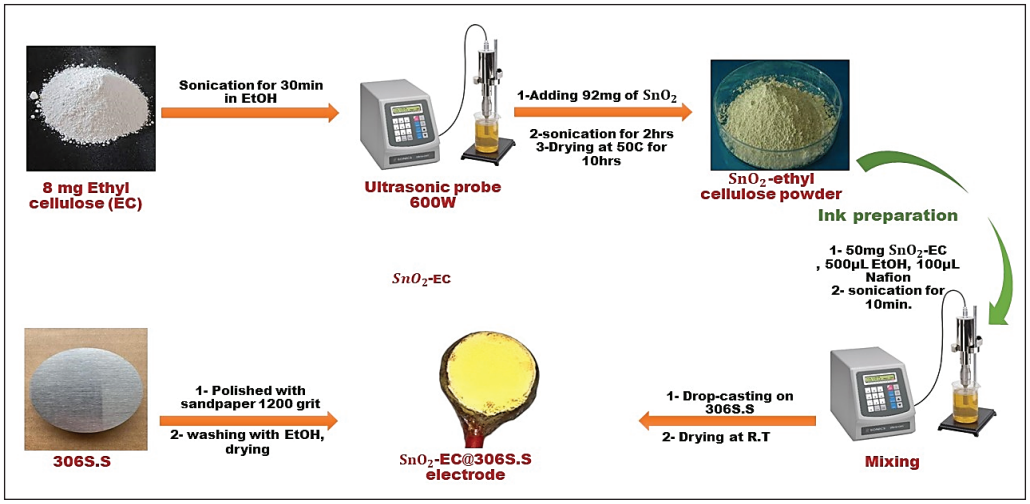

Fig. 1. Illustrate the route of electrocatalyst and ink preparation

2.5. Electrochemical Measurements

Experiments were carried out to reduce CO_2 using an H-type electrochemical cell. A Nafion 117 proton exchange membrane separated the cathodic and anodic compartments. A three-electrode system was used with the electrocatalyst deposited on 306 stainless steel, which served as the working electrode, a high-surface-area platinum plate as the counter electrode (area = 1 cm^2), and a $Hg/HgCl_2$ (saturated KCl) as the reference electrode, as shown in Figure 2. All electrochemical experiments were conducted using a Potentiostat (Vertex One, Ivium Technologies, Netherlands).

The cathodic and anodic compartments were filled with a fresh solution of 110 mL of 0.1M $KHCO_3$. The pH of the catholyte solution was initially measured to be 8.45 before purging with CO_2 gas. After saturating the solution with CO_2 for 60 minutes, the pH decreased to 7.23. This significant change in pH demonstrates the strong influence of CO_2 on the solution's acidity. Linear sweep voltammetry (LSV) curves were conducted in an N_2 and CO_2-saturated electrolyte at a flow rate of 10 mL per seconds with an applied potential in the range of 0 to -2 V vs. RHE with a scan rate of 10 mV per seconds. All potentials were calibrated against the reversible hydrogen electrode (RHE) using Equation1.

$$E_{RHE} = V_{SCE} + 0.24 + 0.0592 \times pH \quad \text{(Eq.1)}$$

Electrochemical impedance spectroscopy (EIS) was carried out under the same electrolyte and electrodes with an amplitude of 10 mV and a frequency ranging from 0.1 Hz to 100 kHz at AC potential.

3. Result and Discussion

3.1. Morphology Characterization

The FE-SEM equipped with EDX was used to characterize the morphology of SnO_2 nanoparticles and ethyl cellulose doped with SnO_2 nanoparticles, as shown in Figures (3A and 3B). The microscopic images of SnO_2 nanoparticles at low (50kx) and high (100kx) magnifications, as displayed in Figure 3A, clearly demonstrate that the particles exhibit a uniform spherical shape with a diameter ranging from 12.67nm to 16.20nm. Furthermore, the surface appeared rougher due to the small sizes of the SnO_2 nanoparticles.

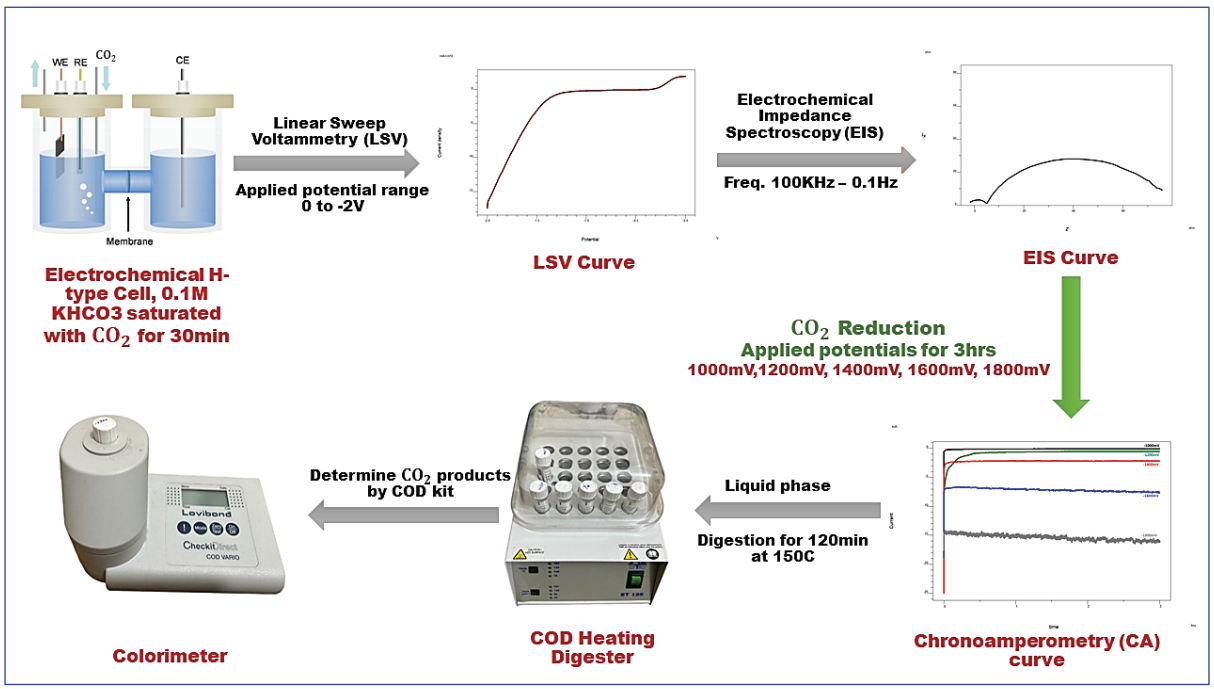

Fig. 2. Electrochemical measurement steps using an H-type cell with three electrode systems

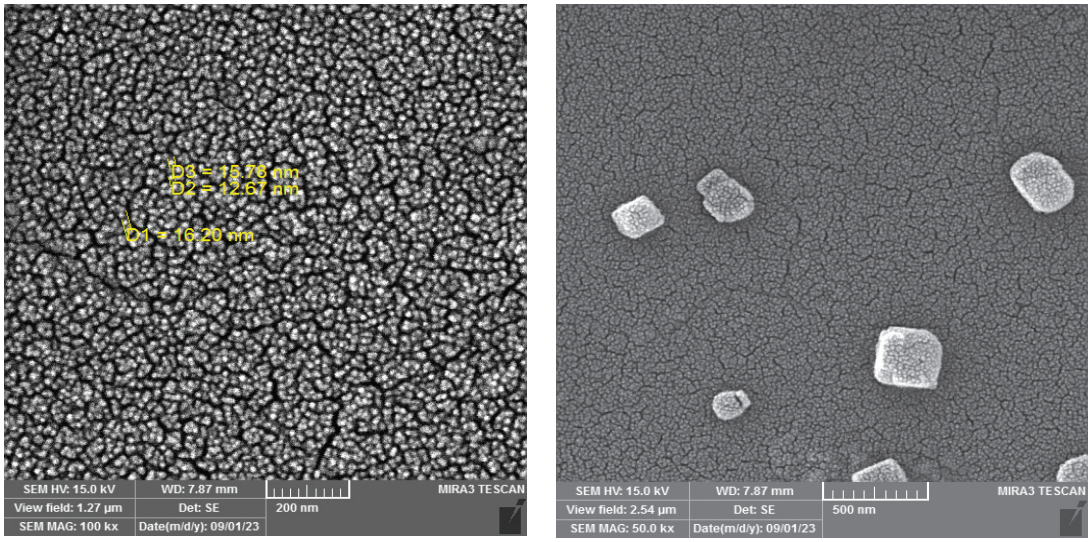

Fig. 3A. FESEM images of SnO_2 nanoparticles with low (left) and high (right) magnification**.**

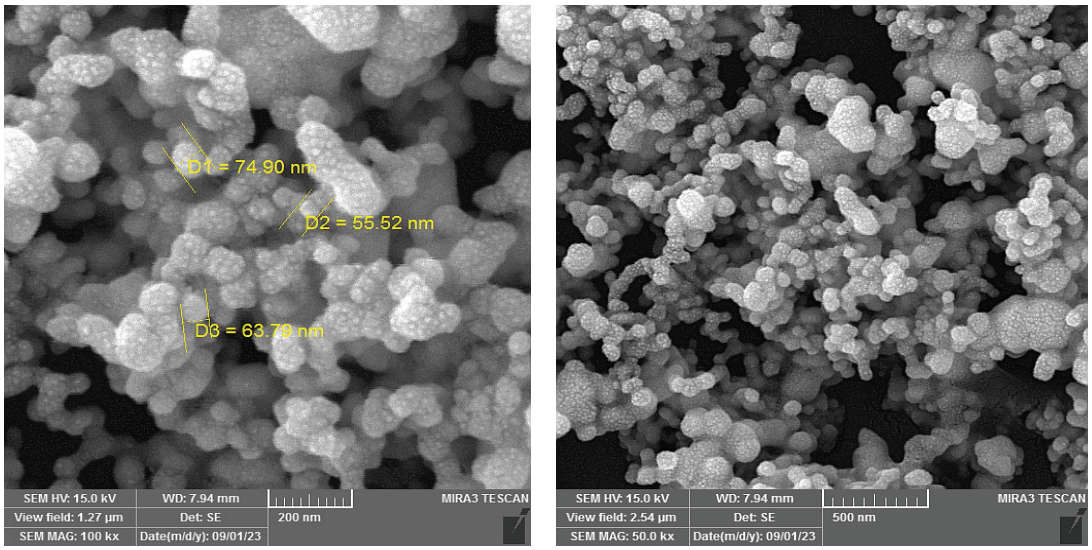

Fig. 3B. FESEM images of SnO_2 NPs-doped ethyl cellulose as clusters

Doping SnO_2 nanoparticles into ethyl cellulose (EC) resulted in individual nanoparticle clusters, each containing more than ten particles. The stiffening action of ethyl cellulose improves the surface adherence of SnO_2 nanoparticles, which causes the size of the particles to increase and become variable, ranging from 55.52 nm to 74.90 nm, as shown in Figure 3B.

3.2. AFM Characterization

An atomic force microscope (AFM) is a technique that provides two and three-dimensional high-resolution images that result in information about topography and morphology. In brief, all prepared electrodes were measured in tapping mode, the most common dynamic mode type used in AFM. In this mode, the cantilever (Tap300-G, reflected coating with 30nm Au, Resonance freq. 300KHz and force constant 42N/m) oscillated with its resonance frequency near the surface. The SnO_2@306S.S electrode with scanned area (2 × 2um) observed spherical-like shapes with uniform distribution of SnO_2 nanoparticles over 306S.S surface, while ethyl cellulose doped with SnO_2 NPs demonstrated aggregation of SnO_2 NP within EC layer that led to increase particle size as

compared with pure SnO_2 NPs which was shown in Figure 4. Regarding surface roughness, the SnO_2-EC@306S.S electrode exhibited higher roughness than the SnO2@306S.S electrode; the mean diameter, root mean square height (Sq), and surface roughness (Sa) calculated using SPIP mountains software are listed in Table 2.

Force-distance (FD) spectroscopy is an AFM mode that can measure the nano-mechanical properties of various materials, such as adhesion force, hardness, adhesion energy, and work function. The force-distance curve is obtained by allowing the cantilever tip to approach the sample surface, leading to an attractive force (Van der Waals forces). When the tip comes into contact with the surface, a rise in repulsive force (electrostatic forces) occurs, pushing the tip away from the surface and causing the cantilever to bend to overcome the tip-sample adhesion forces. The tip is then pulled sharply toward its equilibrium position, and the value of tip-surface deflection is monitored and recorded as a function of tip-surface displacement [32-35] as illustrated in Figure 5. This data is then plotted as a force-distance curve, which is used to estimate the adhesion force (pull-off force).

The force-distance curve of the SnO_2-EC@306S.S

Table 2. Mean diameters, root mean square height (Sq), and surface roughness (Sa) of prepared catalyst.

No.	Electrode	Sq (nm)	Sa (nm)	Mean diameter (nm)
1	SnO2@306S.S	7	5	31.29
2	SnO2-EC@306S.S	56	35	98.30

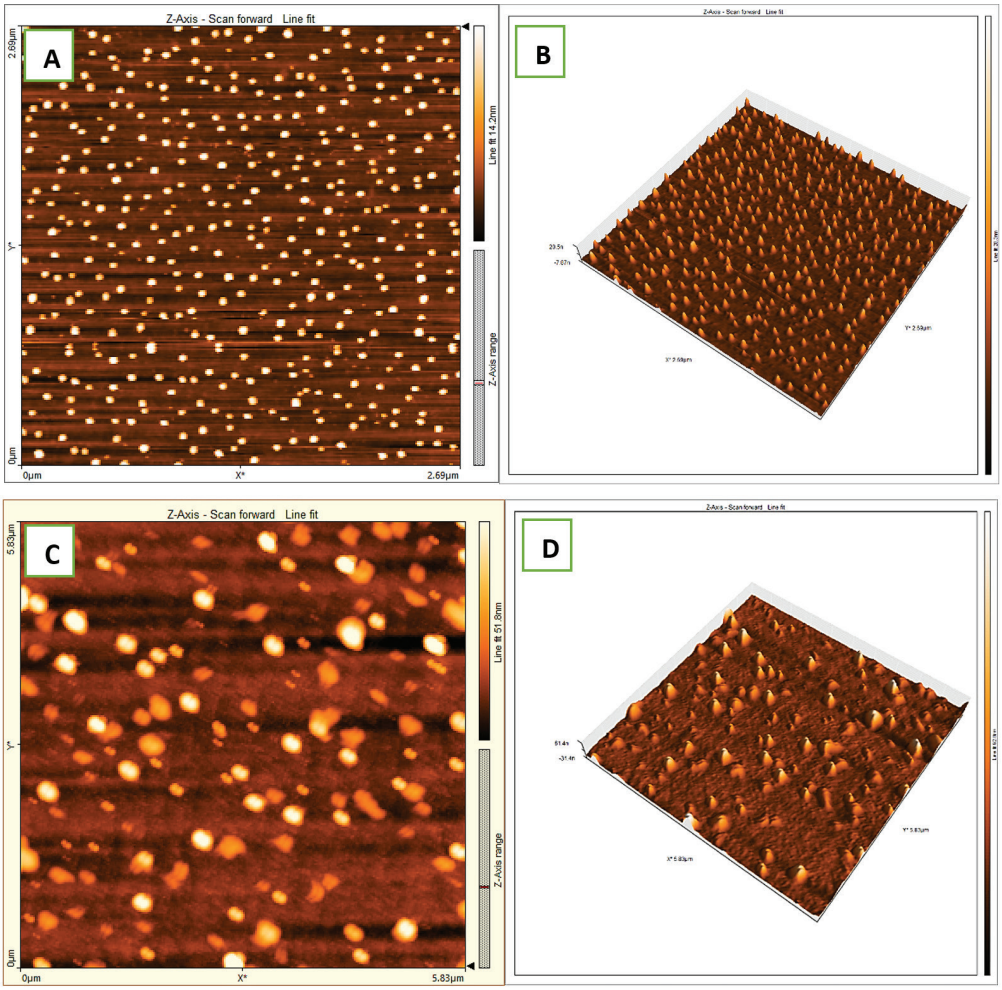

Fig. 4. 2D and 3D-dimensional of SnO_2 NPs (A, B) SnO_2 NPs-doped ethyl cellulose (C, D)

electrode showed a large pull-off force of 0.519 nN and a hardness of 1.601 MPa. In contrast, the SnO_2@306S.S electrode exhibited a lower adhesion force of 0.093 nN and a hardness of 52 kPa, as depicted in Figure 6. The higher adhesion value of the SnO_2-EC@306S.S electrode may be attributed to the presence of OH-groups in the structure of ethyl cellulose, which plays an important role in holding SnO_2 NPs on the stainless-steel surface through hydrogen bonding with vapour water, making the surface hydrophilic. Therefore, more force is required to pull the tip away from the surface. Additionally, the higher surface roughness of the SnO_2-EC@306S.S electrode resulted in a higher adhesion force compared to the lower roughness of the SnO_2@306S.S electrode. All force-distance spectroscopy measurements were conducted in contact mode in an air environment, using a cantilever with a backside aluminium reflective coating (30 nm), a force constant of 0.2N/m, a frequency of 13 KHz, and a tip radius of 10nm.

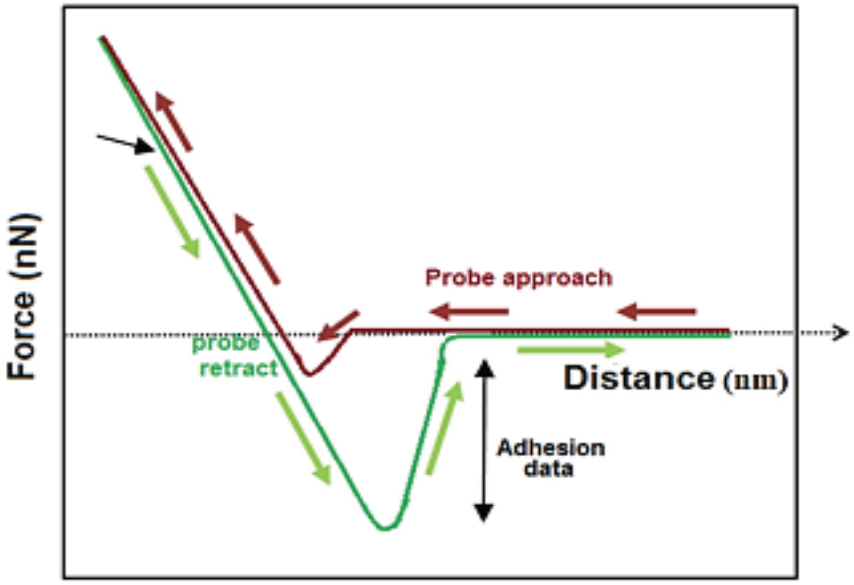

Fig. 5. Diagram of force–distance curve [35]

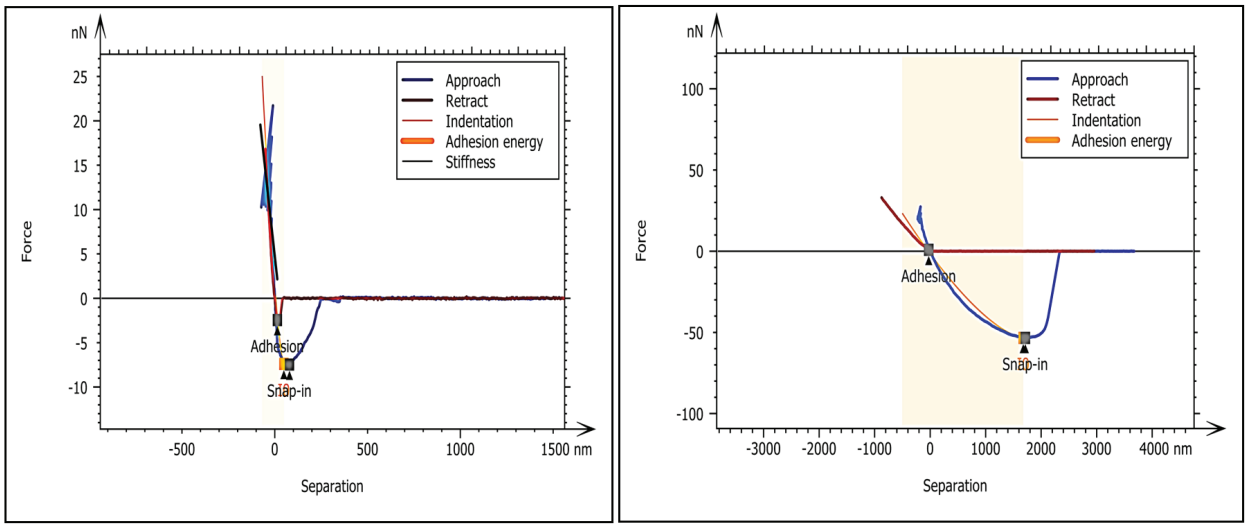

Fig. 6. Force-distance curve of SnO_2-EC@306SS (left) and of SnO_2@306SS (right) electrodes.

3.3. X-Ray Diffraction Analysis

The diffractograms for both sonicated ethyl cellulose (EC) and SnO_2-doped ethyl cellulose as shown in Figure 7. Ethyl cellulose pattern showed a broad peak at a position of 17.06°, corresponding to a d-spacing of 0.5193 nm. This broad peak could be attributed to the amorphous structure and nano-size effect after treatment with an ultrasonic probe for 60 minutes.

The average crystalline size was calculated using the Debye-Scherer formula [36-40] as illustrated in Equation 2 and was found to be 45 nm.

$$D = \frac{0.9\,\lambda}{\beta\,COS\theta} \qquad \text{(Eq.2)}$$

Where D is the crystalline grain size, B = FWHM, = angle of diffraction and = wavelength of x-ray. The XRD pattern of SnO_2-doped ethyl cellulose powder displayed more than ten peaks with different intensities and positions listed in the Table 3. The narrow and sharp diffraction peaks revealed no impurities in the prepared catalyst, indicating good crystallinity. The average size estimated to be 44.21 nm, which is in close agreement with results obtained by FESEM and AFM.

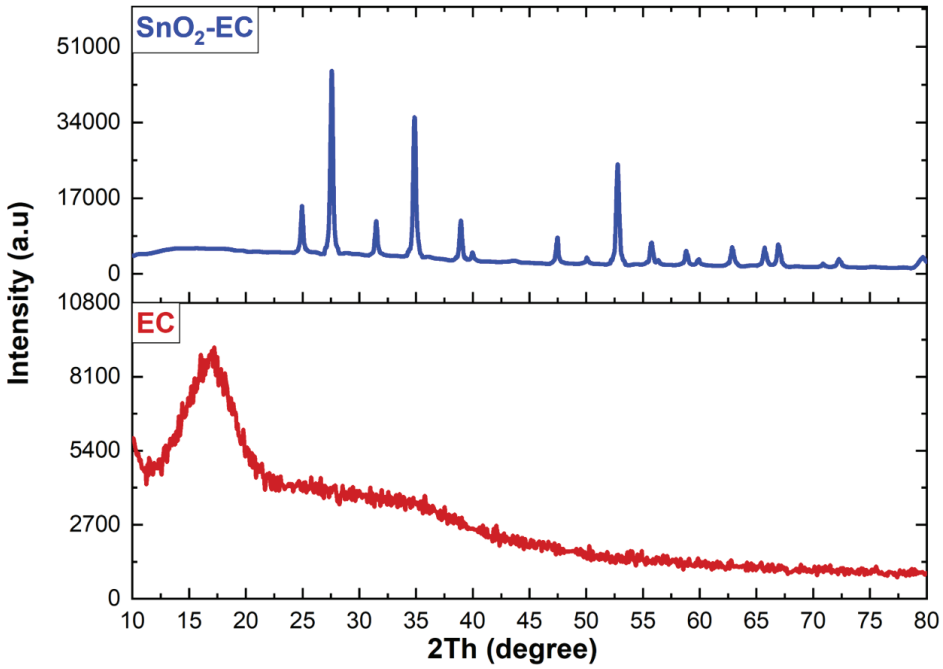

Fig. 7. XRD pattern of ethyl cellulose (EC) and SnO_2-doped EC.

Table 3. XRD parameters of SnO_2-doped ethyl cellulose

No.	FWHM [°2Th]	Peak pos. [°2Th]	Crystallite size (nm)	No	FWHM [°2Th]	Peak pos. [°2Th]	Crystallite size (nm)
1	0.197	24.944	43.0	8	0.216	55.975	43.3
2	0.108	27.540	81.8	9	0.276	58.794	34.0
3	0.177	31.470	48.8	10	0.236	59.913	40.2
4	0.197	34.822	44.1	11	0.236	62.880	40.8
5	0.216	38.966	40.5	12	0.276	65.696	35.3
6	0.197	47.488	45.9	13	0.236	66.921	41.8
7	0.187	52.782	49.5	14	0.336	72.250	30.0

3.4. Electrochemical Performance

Conducted linear sweep voltammetry tests on three electrodes (306S.S, EC@306S.S, and SnO_2-EC@306S.S) in 0.1M $KHCO_3$ electrolytes saturated with N_2 and CO_2, in the voltage range of 0 to -2V (Fig.8). The onset potential for all three electrodes was -1V, indicating stability within the applied potential range. In CO_2-saturated conditions, the current densities for both electrodes (306S.S and EC/306S.S) were measured at -5 mA/cm^2 and -8 mA/cm^2, respectively. This suggests that the use of rotated disc and ethyl cellulose loaded on 306 stainless steels did not contribute to ECO_2RR due to low current densities. From the LSV curve, we observed that the SnO_2-EC@306S.S electrocatalyst exhibited a significant increase in current density in CO_2-saturated electrolytes, reaching -33 mA cm^{-2}, compared to -0.205 mA cm^{-2} in N_2-saturated conditions. This indicates lower current density in the absence of CO_2 (N_2-saturated) due to hydrogen production from the hydrogen evolution reaction (HER) in the cathodic region, which is considered a side product competing with CO_2RR and reduces faradaic efficiency. The higher current density contributes to CO_2 reduction and HER, demonstrating that the prepared catalyst is more electrically active towards CO_2 electrochemical reduction despite the production of H_2 gas.

The double layer capacitances (Cdl) and charge transfer resistance (Rct) parameters of 306S.S, EC/306S.S, and SnO_2-EC/306S.S electrodes were estimated after fitted electrical equivalent circuit using the electrochemical impedance spectroscopy technique at a potential of -1.2V vs RHE, as listed in Table 4. The Nyquist plot resulting from the EIS investigation shows a smaller semicircle due to the higher conductivity of the SnO_2-EC/306S.S electrode. The 306S.S electrode exhibited a low Cdl

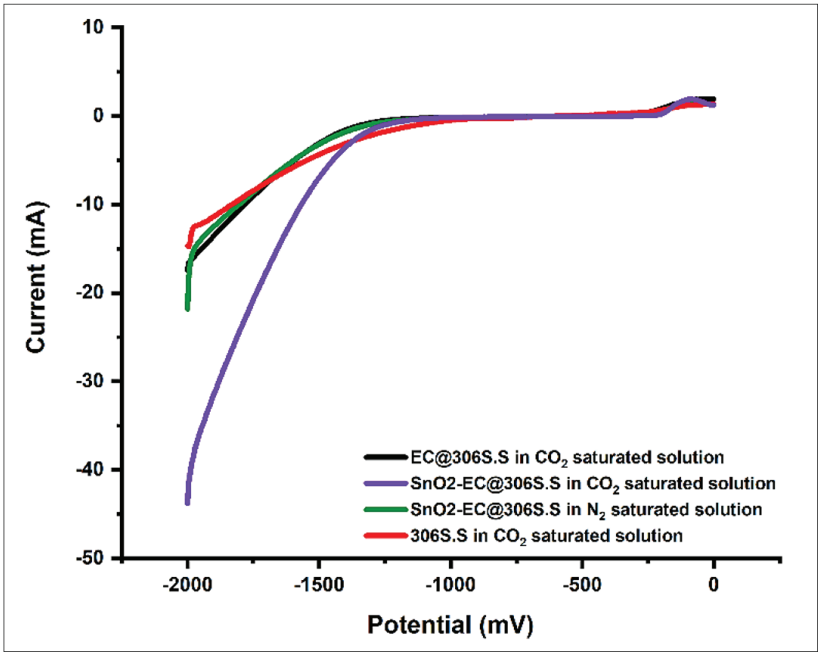

Fig. 8. Linear sweep voltammograms of 306S.S, EC@306S.S, and SnO_2-EC@306S.S in 0.1M $KHCO_3$ electrolyte saturated with N_2 and CO_2 gas.

Table 4. Charge transfer resistance (R_{ct}) and double layer capacitance (C_{dl}) of prepared electrodes

Electrode	Charge transfer resistance Rct (ohm)	Double layer capacitances C_{dl} (F cm^{-2})
SnO_2-EC/306S.S	5.519E+01	6.432E-04
EC/306S.S	5.902E+01	6.421E-04
306S.S	6.157E+01	6.412E-04

(0.0006412 F cm^{-2}), followed by EC/306S.S, which showed a slight increase in Cdl (0.0006421 Fcm^{-2}). However, the SnO_2-EC/306S.S electrocatalyst showed a higher Cdl (0.0006432 F cm^{-2}) as illustrated in Figure 9. The higher value of Cdl indicates that the catalyst has a high electrochemically active surface area (ECSA) and more active sites in the SnO_2-EC/306S.S catalyst, which leads to enhanced electrocatalytic activity of the desired electrode for the CO_2 reduction reaction. The higher conductivity of the SnO_2-EC/306S.S electrocatalyst could be attributed to the lower charge transfer resistance (Rct 5519 ohm) that improves electrocatalytic CO_2 reduction, while electrodes 306S.S and EC/306S.S exhibited high Rct (low conductivity).

The electrocatalytic performance of the SnO_2-EC/306S.S electrode was investigated using chronoamperometry to determine the oxygen content of products under different applied potentials (ranging from -1 to -1.8 mV) for 180 minutes at each potential in a 0.1M $KHCO_3$ solution saturated with CO_2 gas, as shown in Figure 10. The current density of the SnO_2-EC/306S.S electrode increased with the increase in applied potential and remained constant without any drop during CO_2 reduction, indicating its good stability.

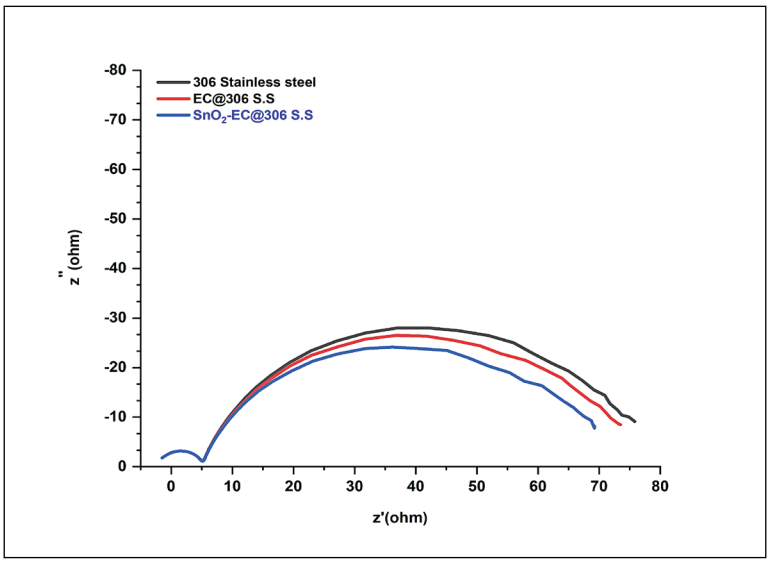

Fig. 9. Nyquist plots of 306S.S, EC@306S.S, and SnO_2-EC@306S.S in 0.1M $KHCO_3$ electrolyte saturated with CO_2 gas

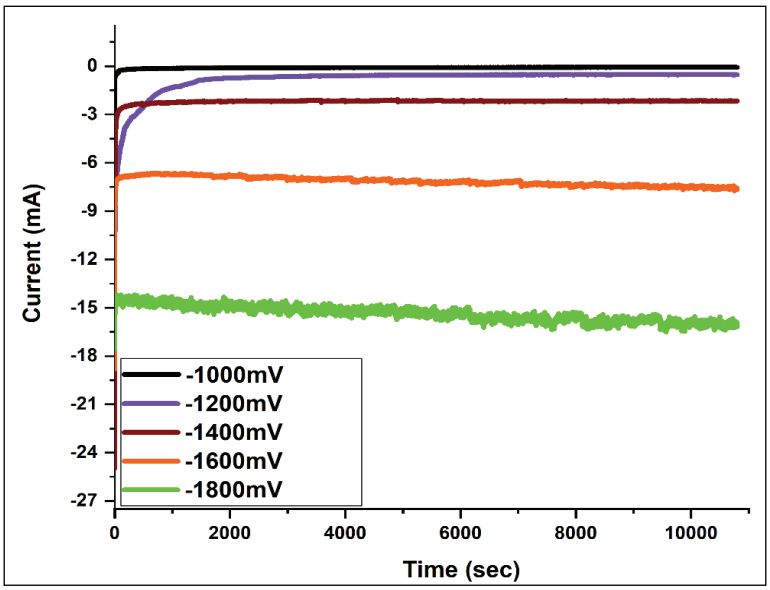

Fig. 10. Chronoamperometry curves at different applied potentials for 3 hrs.

The liquid products at each potential are collected and analysed using a chemical oxygen demand (COD) test. This method is used to detect the amount of oxidizable organic compounds in liquid and waste based on the reduction of potassium dichromate (K_2CrO_7) to chromium salt at high temperatures reaching 150°C [41]. The absorbance is then determined using a colorimeter as shown in Figure 11.

The SnO_2-EC/306S.S electrode demonstrated high electrocatalytic performance with a high oxygen content at an applied potential of -1.2V vs. RHE (-2mA cm^{-2}) and a concentration of 235 mgL^{-1}. This was indicated by a colour change in the dichromate from yellow to black, showing the oxidation of organic products. As the potential increased towards the more negative cathodic region, the oxygen content decreased, measuring 46 mgL^{-1}, 31 mgL^{-1}, and 17 mgL^{-1} for potentials of -1.4V vs. RHE (-2 mA cm^{-2}), -1.6V vs. RHE (-7.3 mA cm^{-2}), and -1.8V vs. RHE (-15.6 mA cm^{-2}), respectively. This suggests that high potentials were not favorable for CO_2 reduction due to the competing hydrogen evolution reaction (HER), leading to a decrease in oxygen content in the liquid products. The COD test indicated no reduction process at a potential of -1V vs. RHE (-0.7 mA cm^{-2}) when CO_2 reduction occurred at a less harmful potential, as listed in Table 5.

Fig 11. Colour of oxidized CO_2 products at different applied potentials

Table 5. Oxygen content of CO_2 products at different applied potentials

No	Potential (mV)	Current (mA cm^{-2})	Temp. (^oC)	COD (mg L^{-1})	Colour
1	Blank	----	25	----	Yellow
2	-1000	0.7	25	0	Yellow
3	-1200	2.0	25	235	Black
4	-1400	2.5	25	46	Yellow
5	-1600	7.3	25	31	Yellow
6	-1800	15.6	25	17	Yellow

4. Conclusion

This study doped SnO_2 nanoparticles (30 nm) with ethyl cellulose ultrasonically to enhance their adhesion to a rotated disc made of 306S.S. This was done to prevent degradation of the catalyst-coated layer in the electrolyte during CO_2 reduction. Ethylcellulose played a key role by making the SnO_2 nanoparticles more rigid, resulting in increased hardness from 52 kPa to 1.601 MPa and surface roughness from 5 nm to 35 nm. Electrochemical CO_2 reduction using a three-electrode setup was performed in a 0.1 M $KHCO_3$ solution saturated with CO_2. Among the three electrodes tested (306S.S., EC@306S.S., and SnO_2-EC@306S.S.), only SnO_2-EC@306S.S. exhibited a high current density of -33 mA cm^{-2} via LSV. This was due to its low charge transfer resistance (Rct 5519 ohm) and high electrical conductivity (Cdl 0.0006432 F cm^{-2}), making it a well-suited electrode for the CO_2 reduction reaction. The electrode also showed high oxygen demand through COD testing at a potential of -1.2V, estimated at 235 mg L^{-1}.

5. Acknowledgements

This research is reinforced by Chemical Analysis Centre (CAC), Baghdad, Iraq

6. References

[1] M. Rumayor Villamil, A. Domínguez Ramos, J.Á. Irabien Gulías, Formic acid manufacture: carbon dioxide utilization alternatives, Appl. Sci. *8* (2018) 914. https://doi.org/10.3390/app8060914

[2] J. Qiao, Y. Liu, F. Hong, J.J.C.S.R. Zhang, A review of catalysts for the electroreduction of carbon dioxide to produce low-carbon fuels, Chem. Soc. Rev., 43 (2014) 631-675. https://doi: 10.1039/c3cs60323g

[3] M. Schreier, F. Héroguel, L. Steier, S. Ahmad, J.S. Luterbacher, M.T. Mayer, J. Luo, M.J.N.E. Grätzel, Solar conversion of CO_2 to CO using Earth-abundant electrocatalysts prepared by atomic layer modification of CuO, Nat. Energy, 2 (2017) 17087. https://doi.org/10.1038/nenergy.2017.87

[4] N. Mozaffari, Alireza Haji Seyed Mirzahosseini, and Niloofar Mozaffari. A new kinetic models analysis for CO adsorption on palladium zeolite nanostructure by roll-coating technique, Anal. Method Environ. Chem. J., 3 (2) (2020) 92-107. https://doi.org/10.24200/amecj.v3.i02.106

[5] Y. Zhang, X. Su, L. Li, H. Qi, C. Yang, W. Liu, X. Pan, X. Liu, X. Yang, Y.J.A.C. Huang, Ru/TiO_2 catalysts with size-dependent metal/support interaction for tunable reactivity in Fischer–Tropsch synthesis, ACS Catal., 10 (2020) 12967-12975. https://doi.org/10.1021/acscatal.0c02780

[6] J. Kang, S. He, W. Zhou, Z. Shen, Y. Li, M. Chen, Q. Zhang, Y.J.N.c. Wang, Single-pass transformation of syngas into ethanol with high selectivity by triple tandem catalysis, Nat. Commun., 11 (2020) 827. https://doi: 10.1038/s41467-020-14672-8

[7] W.-H. Wang, Y. Himeda, J.T. Muckerman, G.F. Manbeck, E.J.C.r. Fujita, CO_2 hydrogenation to formate and methanol as an alternative to photo and electrochemical CO_2 reduction, Chem. Rev., 115 (2015) 12936-12973. https://doi: 10.1021/acs.chemrev.5b00197

[8] W. Li, H. Wang, X. Jiang, J. Zhu, Z. Liu, X. Guo, C.J.R.a. Song, A short review of recent advances in CO_2 hydrogenation to hydrocarbons over hetero-geneous catalysts, RSC Adv., 8 (2018) 7651-7669. https://doi.org/10.1039/C7RA13546G

[9] R. Kortlever, I. Peters, S. Koper, M.T.J.A.C. Koper, Electrochemical CO_2 reduction to formic acid at low overpotential and with high faradaic efficiency on carbon-supported bimetallic Pd–Pt nanoparticles, ACS Catal., 5 (2015) 3916-3923. http://dx.doi.org/10.1021/acscatal.5b00602

[10] A.A. Miran Beigia, Mojtaba Shamsipur, Biochemistry Method: Simultaneous determination of formaldehyde and methyl

tert-buthyl ether in water samples using static headspace gas chromatography mass spectrometry, Anal. Method Environ. Chem. J., 2 (2019) 33-42. https://doi.org/10.24200/amecj.v2.i01.40

[11] X. Zhang, T. Lei, Y. Liu, J.J.A.C.B.E. Qiao, Enhancing CO_2 electrolysis to formate on facilely synthesized Bi catalysts at low overpotential, Appl. Catal. B: Environ., 218 (2017) 46-50. https://doi.org/10.1016/j.apcatb.2017.06.032

[12] Y. Li, Y. Li, Y. Wan, Y. Xie, J. Zhu, H. Pan, X. Zheng, C.J.A.E.M. Xia, Perovskite oxyfluoride electrode enabling direct electrolyzing carbon dioxide with excellent electrochemical performances, Adv. Energy Mater., 9 (2019) 1803156. http://dx.doi.org/10.1002/aenm.201803156

[13] M. Ma, K. Djanashvili, W.A.J.A.c.i.e. Smith, Controllable hydrocarbon formation from the electrochemical reduction of CO_2 over Cu nanowire arrays, Angewandte Chem., 55 (2016) 6680-6684. https://doi.org/10.1002/anie.201601282

[14] B. Parsazadeh, H. Asilian Mahabadi, N. Damyar, Removal and determination of carbon monoxide based on copper oxide immobilized on Zeolite 13X Nanocatalyst by catalytic oxidation process and gas flow analyzer, Anal. Method Environ. Chem. J., 6 (2023) 37-51. https://doi.org/10.24200/amecj.v6.i04.259

[15] Z. Weng, J. Jiang, Y. Wu, Z. Wu, X. Guo, K.L. Materna, W. Liu, V.S. Batista, G.W. Brudvig, H.J.J.o.t.A.C.S. Wang, Electrochemical CO_2 reduction to hydrocarbons on a heterogeneous molecular Cu catalyst in aqueous solution, J. Am. Chem. Soc., 138 (2016) 8076-8079. https://doi.org/10.1021/jacs.6b04746

[16] Y.Y. Birdja, J.J.C. Vaes, Towards a critical evaluation of electrocatalyst stability for CO_2 electroreduction, Chem. Electro. Chem., 7 (2020) 4713-4717. https://doi.org/10.1002/celc.202001227

[17] G. Centi, S. Perathoner, G. Winè, M.J.G.C. Gangeri, Electrocatalytic conversion of CO_2 to long carbon-chain hydrocarbons, Green Chem., 9 (2007) 671-678. https://doi.org/10.1039/B615275A

[18] M. Gattrell, N. Gupta, A.J.J.o.e.C. Co, A review of the aqueous electrochemical reduction of CO_2 to hydrocarbons at copper, J. Electroanal. Chem., 594 (2006) 1-19. https://doi.org/10.1016/j.jelechem.2006.05.013

[19] D.T. Whipple, P.J.J.T.J.o.P.C.L. Kenis, Prospects of CO_2 utilization via direct heterogeneous electrochemical reduction, J. Phys. Chem. Lett., 1 (2010) 3451-3458. https://doi.org/10.1021/jz1012627

[20] A. á Loiudice, P. á Lobaccaro, E. á Kamali, T. á Thao, B.J.A.C. á Huang, Int. Ed, JW áAger, R. áBuonsanti, Tailoring Copper Nanocrystals towards C_2 Products in Electrochemical CO_2 Reduction, Angewandte Chem., 55 (2016) 5789. https://doi.org/10.1002/anie.201601582

[21] H.-K. Lim, H. Shin, W.A. Goddard III, Y.J. Hwang, B.K. Min, H.J.J.o.t. A.C.S. Kim, Embedding covalency into metal catalysts for efficient electrochemical conversion of CO_2, J. Am. Chem. Soc., 136 (2014) 11355-11361. https://doi.org/10.1021/ja503782w

[22] D. Kim, J. Resasco, Y. Yu, A.M. Asiri, P.J.N.c. Yang, Synergistic geometric and electronic effects for electrochemical reduction of carbon dioxide using gold–copper bimetallic nanoparticles, Nat. Commun., 5 (2014) 4948. https://doi.org/10.1038/ncomms5948

[23] A.S. Agarwal, Y. Zhai, D. Hill, N.J.C. Sridhar, The electrochemical reduction of carbon dioxide to formate/formic acid: engineering and economic feasibility, ChemSusChem., 4 (2011) 1301-1310. https://doi.org/10.1002/cssc.201100220

[24] Y. Hori, H. Wakebe, T. Tsukamoto, O.J.E.A. Koga, Electrocatalytic process of CO selectivity in electrochemical reduction

of CO_2 at metal electrodes in aqueous media, Electrochim. Acta, 39 (1994) 1833-1839. https://doi.org/10.1016/0013-4686(94)85172-7

[25] H. Asdollahzadeh, Development of electrochemical sensor based on carbon paste electrode modified with ZnO nanoparticles for determination of chlorpheniramine maleate, Anal. Method Environ. Chem. J., 4 (2021) 16-25. https://doi.org/10.24200/amecj.v4.i01.130

[26] K. Ibrahim Alabid, and Hajar Naser Nasser, Determine methylene blue based on carbon paste electrode modified with nanoparticles of nickel oxide-nitrogen carbon quantum dots and carbon structures by cyclic voltammetry, Anal. Method Environ. Chem. J., 7 (2024) 17-29. https://doi.org/10.24200/amecj.v7.i01.272

[27] X. Hou, Y. Cai, D. Zhang, L. Li, X. Zhang, Z. Zhu, L. Peng, Y. Liu, J.J.J.o.m.c.A. Qiao, 3D core–shell porous-structured Cu@Sn hybrid electrodes with unprecedented selective CO_2-into-formate electroreduction achieving 100%, J. Mater. Chem. A, 7 (2019) 3197-3205. https://doi.org/10.1039/C8TA10650A

[28] X. Bai, W. Chen, C. Zhao, S. Li, Y. Song, R. Ge, W. Wei, Y.J.A.C. Sun, Exclusive formation of formic acid from CO_2 electroreduction by a tunable Pd-Sn alloy, Angewandte Chem., 129 (2017) 12387-12391. https://doi.org/10.1002/anie.201707098

[29] T. Lai, K. Shi, P.J.T.J.o.A. Huang, Adhesion force behaviors between two silica surfaces with varied water thin film due to substrate temperature studied by AFM, J. Adhesion, 96 (2020) 855-872. https://doi:10.1080/00218464.2018.1523725

[30] M. N. Jassim, Z. S. Rasheed, Enhancement optical characterized of tin oxide in polymer polyvinyl alcohol colloid prepared by laser ablation method, Baghdad Sci. J., 21 (2024) 2425-2425. https://doi.org/10.21123/bsj.2023.8494

[31] A. Alwash, The green synthesize of zinc oxide catalyst using pomegranate peels extract for the photocatalytic degradation of methylene blue dye, Baghdad Sci. J., 17 (2020) 0787-0787. https://doi.org/10.21123/bsj.2020.17.3.0787

[32] M. Trought, K.A.J.J.o.C.E. Perrine, Investigating the relationship between adhesion forces and surface functionalization using atomic force microscopy, J. Chem. Educ., 98 (2021) 1768-1775. http://dx.doi.org/10.1021/acs.jchemed.0c00558

[33] K. Ono, Y. Mizushima, M. Furuya, R. Kunihisa, N. Tsuchiya, T. Fukuma, A. Iwata, A.J.A. Matsuki, Direct measurement of adhesion force of individual aerosol particles by atomic force microscopy, Atmosphere, 11 (2020) 489. https://doi.org/10.3390/atmos11050489

[34] S. Sadegh Hassani, M. Daraee, Z.J.J.o.A.S. Sobat, Technology, Application of atomic force microscopy in adhesion force measurements, J. Adhesion Sci. Technol., 35 (2021) 221-241. http://dx.doi.org/10.1080/01694243.2020.1798647

[35] R. Sharma, V. Kumar, Y.J.C.l. Goswami, Excellent flexible Tin Oxide-metal sulfide nanocomposites grown by spin coating chemical route, Chalcogenide Lett., 18 (2021) 473-479. http://dx.doi.org/10.15251/CL.2021.188.473

[36] T. Kondo, Y. Tamura, M. Hoshino, T. Watanabe, T. Aikawa, M. Yuasa, Y.J.A.c. Einaga, Direct determination of chemical oxygen demand by anodic decomposition of organic compounds at a diamond electrode, Anal. Chem., 86 (2014) 8066-8072. https://doi.org/10.1021/ac500919k

[37] S. A. Hamdan, Characterization study of neodymium doped Tin oxide films for optoelectronic applications, Iraqi J. Sci., 65 (2024) 2479-2489. https://doi.org/10.24996/ijs.2024.65.5.12

[38] A. Nada Mohammed, A. A. Baqer, A selective NH3 gas sensor based on (Ag_2O) 1-x (SnO_2) x nanocomposites thin films at various operating temperatures, Baghdad Sci. J., 21 (2024) 1391-1391. https://doi.org/10.21123/bsj.2023.8117

[39] M. K. Alshujery, K. Abid Saleh Al-Saadie, Anodizing of aluminum 6061 alloy with incorporated nanoparticles to inhibits the aluminum corrosion, Int. J. Health Sci., 6 (2022) 930-940. https://doi.org/10.53730/ijhs.v6nS1.4847

[40] M. M. Abbas, A. Ab-M. Shehab, N. A. Hassan, A. K. Al-Samuraee, Effect of temperature and deposition time on the optical properties of chemically deposited nanostructure PbS thin films, Thin Solid Films, 519 (2011) 4917-4922. https://doi.org/10.1016/j.tsf.2011.01.053

[41] A.E. Rodríguez-Mata, L.E. Amabilis-Sosa, A. Roé-Sosa, J.M. Barrera-Andrade, J.G. Rangel-Peraza, Quantification of recalcitrant organic compounds during their removal test by a novel and economical method based on chemical oxygen demand analysis, Korean J. Chem. Eng., 36 (2019) 423-432. http://dx.doi.org/10.1007/s11814-018-0203-9